

# 1 The BackMAP Python Module: How a 2 Simpler Ramachandran Number Can 3 Simplify the Life of a Protein Simulator

4 Ranjan V. Mannige<sup>1,\*</sup>

5 <sup>1</sup> Multiscale Institute, Berkeley Lake, GA 30092, U.S.A.

6 \* ranjanmannige@gmail.com

## 7 ABSTRACT

8 Protein backbones occupy diverse conformations, but compact metrics to describe such conformations  
9 and transitions between them have been missing. This report re-introduces the Ramachandran number  
10 ( $\mathcal{R}$ ) as a residue-level structural metric that could simply the life of anyone contending with large numbers  
11 of protein backbone conformations (e.g., ensembles from NMR and trajectories from simulations).  
12 Previously, the Ramachandran number ( $\mathcal{R}$ ) was introduced using a complicated **closed form**, which  
13 made the Ramachandran number difficult to implement. This report discusses a much simpler closed  
14 form of  $\mathcal{R}$  that makes it much easier to calculate, thereby making it easy to implement. Additionally, this  
15 report discusses how  $\mathcal{R}$  dramatically reduces the dimensionality of the protein backbone, thereby making  
16 it ideal for simultaneously interrogating large number of protein structures. For example, two hundred  
17 distinct conformations can easily be described in one graphic using  $\mathcal{R}$  (rather than two hundred distinct  
18 Ramachandran plots). Finally, a new Python-based backbone analysis tool – BACKMAP – is introduced  
19 that reiterates how  $\mathcal{R}$  can be used as a simple and succinct descriptor of protein backbones and their  
20 dynamics.

## 21 INTRODUCTION

22 Proteins are a class of biomolecules unparalleled in their functionality (Berg *et al.*, 2010). A natural  
23 protein may be thought of as a linear chain of amino acids, each normally sourced from a repertoire of  
24 20 naturally occurring amino acids. Proteins are important partially because of the structures that they  
25 access: the conformations (conformational ensemble) that a protein assumes determines the functions  
26 available to that protein. However, all proteins are dynamic: even stable proteins undergo long-range  
27 motions in its equilibrium state; i.e., they have substantial diversity in their conformational ensemble  
28 (James and Tawfik, 2003b,a; Oldfield *et al.*, 2005; Tokuriki and Tawfik, 2009; Schad *et al.*, 2011; Vértessy  
29 and Orosz, 2011; Mannige, 2014). Additionally, a number of proteins undergo conformational transitions,  
30 without which they may not properly function. Finally, some proteins – intrinsically disordered proteins  
31 – display massive disorder whose conformations dramatically change over time (Uversky, 2003; Fink,  
32 2005; Midic *et al.*, 2009; Espinoza-Fonseca, 2009; Uversky and Dunker, 2010; Tompa, 2011; Sibille and  
33 Bernado, 2012; Kosol *et al.*, 2013; Dunker *et al.*, 2013; Geist *et al.*, 2013; Baruah *et al.*, 2015), and whose

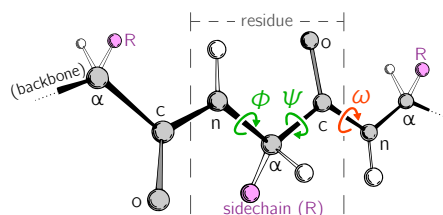


**Figure 1. Backbone conformational degrees of freedom** dominantly depend on the dihedral angles  $\phi$  and  $\psi$  (green), and to a smaller degree depend on the third dihedral angle ( $\omega$ ; red) as well as bond lengths and angles (unmarked).

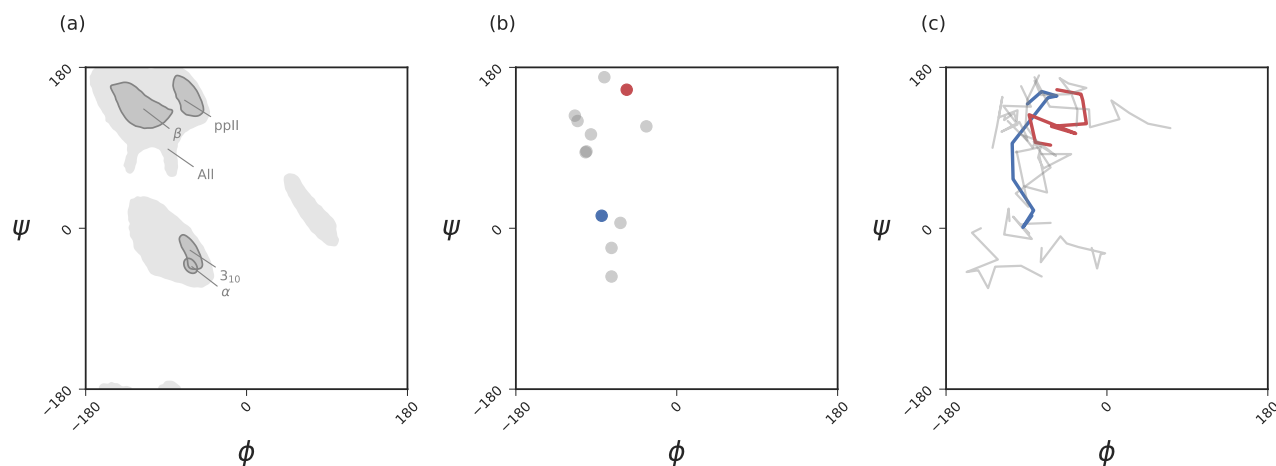


**Figure 2. Ramachandran plots allow for the per-residue representation of backbone conformation. Panel (a) represents regions in the plot that are occupied by backbones describing particular regular secondary structures. Panel (b) represents the positions of a 11 residue peptide that describe, with one dot per residue. Panel (c) represents a seven-frame trajectory, where each residue's backbone traces a line, with** While the Ramachandran plot is useful for getting a *qualitative* sense of peptide backbone structure (a, b), it is not a convenient representation for exploring peptide backbone dynamics (c). Secondary structure keys used here and throughout the document: ‘ $\alpha$ ’ –  $\alpha$ -helix, ‘ $3_{10}$ ’ –  $3_{10}$ -helix, ‘ $\beta$ ’ –  $\beta$ -sheet/extension, ‘ppII’ – polyproline II helix.

34 characteristic structures are still not well-understood (Beck *et al.*, 2008).

35 Large-scale changes in a protein occur due to changes in protein backbone conformations. Fig. 1 is a  
 36 cartoon representation of a peptide/protein backbone, with the backbone bonds themselves represented  
 37 by darkly shaded bonds. Ramachandran *et al.* (1963) had recognized that the backbone conformational  
 38 degrees of freedom available to an amino acid (residue)  $i$  is almost completely described by only two  
 39 dihedral angles:  $\phi_i$  and  $\psi_i$  (Fig. 1, green arrows). **Today, Ramachandran plots are used to qualitatively**  
 40 **describe protein backbone conformations.**

41 The Ramachandran plot is recognized as a powerful tool for two reasons: 1) it serves as a map  
 42 for structural ‘correctness’ (Laskowski *et al.*, 1993; Hoof *et al.*, 1997; Laskowski, 2003), since many  
 43 regions within the Ramachandran plot space are energetically not permitted (Momen *et al.*, 2017); and  
 44 2) it provides a qualitative snapshot of the structure of a protein (Berg *et al.*, 2010; Alberts *et al.*, 2002;  
 45 Subramanian, 2001; Lovell *et al.*, 2003). For example, particular regions within the Ramachandran plot  
 46 indicate the presence of particular secondary locally-ordered structures such as the  $\alpha$ -helix and  $\beta$ -sheet  
 47 (see Fig. 2a).

48 While the Ramachandran plot has been useful as a measure of protein backbone conformation, it is  
 49 not popularly used to assess structural dynamism and transitions (unless specific knowledge exists about  
 50 whether a particular residue is believed to undergo a particular structural transition). This is because  
 51 of the two-dimensionality of the plot: describing the behavior of every residue involves tracking its  
 52 position in two-dimensional ( $\phi, \psi$ ) space. For example, a naive description of positions of a peptide in a  
 53 Ramachandran plot (Fig. 2b) needs more annotations for a per-residue analysis of the peptide backbone’s  
 54 structure. Given enough residues, it would be impractical to track the position of each residue within a  
 55 plot. This is compounded with time, as each point in (b) becomes a curve (c), further confounding the  
 56 situation. The possibility of picking out previously unseen conformational transitions and dynamism  
 57 becomes a logistical impracticality. As indicated above, this impracticality arises primarily from the fact  
 58 that the Ramachandran plot is a two-dimensional map.

59 For example, tracking changes in protein trajectory is either overly detailed or overly holistic: an  
 60 example of an overly detailed study is the tracking on exactly one or a few atoms over time (this  
 61 already poses a problem, since we would need to know exactly which atoms are expected to partake  
 62 in a transition); an example of a holistic metric is the radius of gyration (this also poses a problem,  
 63 since we will never know which residues contribute to a change in radius of gyration without additional  
 64 interrogation). With our understanding of protein dynamics undergoing a new **renaissance** – especially

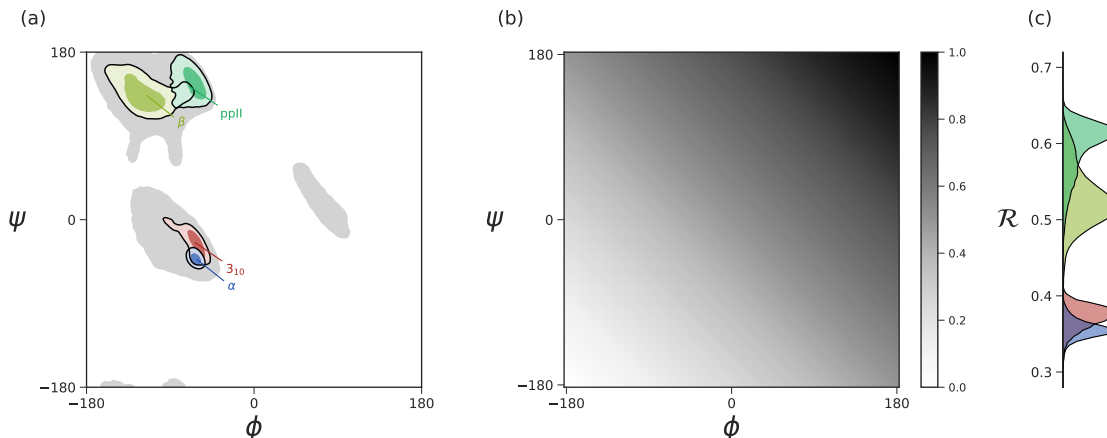


**Figure 3.** Panel (a) describes the distribution of dominant regular secondary structures. Panel (b) shows the mapping between the  $(\phi, \psi)$  and  $\mathcal{R}$ . In particular,  $\mathcal{R}$  increases in negative-sloping sweeps from the bottom left to the top right of the Ramachandran plot. Panel (c) describes the distribution of secondary structures in  $\mathcal{R}$  space. Both Ramachandran plots (a) and Ramachandran ‘lines’ (c) equally resolve the secondary structure space, thereby making  $\mathcal{R}$  a compact yet faithful representation of backbone structure (Mannige *et al.*, 2016).

65 due to intrinsically disordered proteins and allostery – having hypothesis-agnostic yet detailed (residue-  
 66 level) metrics of protein structure has become even more relevant. Consequently, there has been no single  
 67 compact descriptor of protein structure. This impedes the naïve or hypothesis-free exploration of new  
 68 trajectories/ensembles.

69 It has recently been shown that the two Ramachandran backbone parameters  $(\phi, \psi)$  may be conve-  
 70 niently combined into a single number – the Ramachandran number  $[\mathcal{R}(\phi, \psi)$  or simply  $\mathcal{R}]$  – with little  
 71 loss of information (Fig. 3; Mannige *et al.* (2016)). In a previous report, detailed discussions were provided  
 72 regarding the reasons behind and derivation of  $\mathcal{R}$  (Mannige *et al.*, 2016). This report provides a simpler  
 73 version of the equation previously published (Mannige *et al.*, 2016), and further discusses how  $\mathcal{R}$  may be  
 74 used to provide information about protein ensembles and trajectories. Finally, this report introduces a  
 75 software package – BACKMAP – that can be used by to produce **pictograms** that describe the behavior of  
 76 a protein backbone within user-inputted conformations, structural ensembles and trajectories. **Given that**  
 77 **each pictogram provides a picture of the whole protein backbone (i.e., all  $\phi$  and  $\psi$  angles), these**  
 78 **pictograms are named multi-angle pictures (or MAPs).** BACKMAP is presently available on GitHub  
 79 (<https://github.com/ranjanmannige/BackMAP>).

## 80 INTRODUCING THE SIMPLIFIED RAMACHANDRAN NUMBER ( $\mathcal{R}$ )

81 The Ramachandran number is both an idea and an equation. Conceptually, the Ramachandran number ( $\mathcal{R}$ )  
 82 is any closed form that collapses the dihedral angles  $\phi$  and  $\psi$  into one structurally meaningful number  
 83 (Mannige *et al.*, 2016). Mannige *et al.* (2016) presented a version of the Ramachandran number (shown in  
 84 the appendix as Eqn. 7) that was complicated in closed form, **thereby** reducing its utility. Here, a simpler  
 85 and **more** accurate version of the Ramachandran number is introduced. **The appendix** shows how this  
 86 simplified form was derived from the original closed form (Eqns. 7).

Given arbitrary limits of  $\phi \in [\phi_{\min}, \phi_{\max}]$  and  $\psi \in [\psi_{\min}, \psi_{\max}]$ , where the minimum and maximum values differ by  $360^\circ$ , the most general and accurate equation for the Ramachandran number is

$$\mathcal{R}(\phi, \psi) \equiv \frac{\phi + \psi - (\phi_{\min} + \psi_{\min})}{(\phi_{\max} + \psi_{\max}) - (\phi_{\min} + \psi_{\min})}. \quad (1)$$

For consistency, we maintain throughout this paper that  $\phi_{\min} = \psi_{\min} = -180^\circ$  or  $-\pi$  radians, which makes

$$\mathcal{R}(\phi, \psi) = \frac{\phi + \psi + 2\pi}{4\pi}. \quad (2)$$

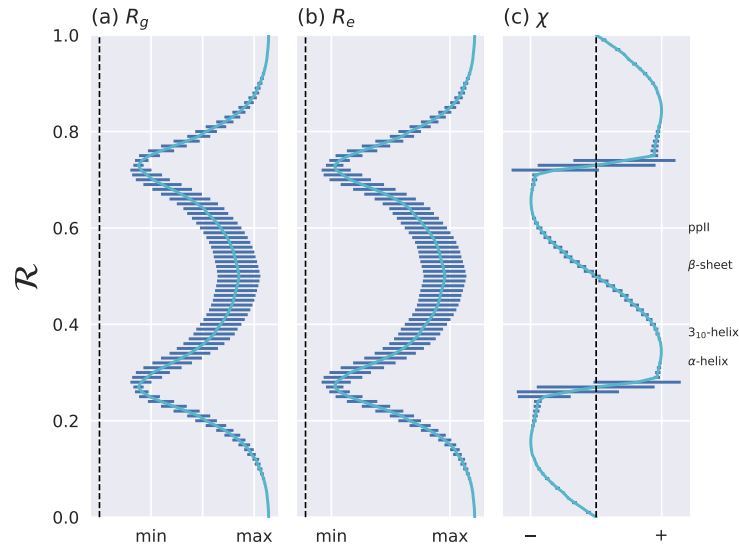


**Figure 4.** The Ramachandran number  $\mathcal{R}$  displays smooth relationships with respect to radius of gyration ( $R_g$ ; a), end-to-end distance ( $R_e$ ; b) and chirality ( $\chi$ ; c), as calculated within Mannige (2017). Light blue lines are average trends, dark blue horizontal lines are error bars. Average positions of dominant structures are shown to the right. These trends explain why  $\mathcal{R}$  is a useful and compact structural measure. Structural measures  $R_g$ ,  $R_e$ , and  $\chi$  were obtained by computationally generating polyglycine peptides of length 10 for all possible  $\phi$  and  $\psi \in [-180, -175, \dots, 175, 180]$ . This was done using the Python library PeptideBuilder (Tien et al., 2013). Values for  $R_g$ ,  $R_e$ , and  $\chi$  were obtained for each peptide and binned with respect to its  $\mathcal{R}(\phi, \psi)$  (each bin represents a region in  $\mathcal{R}$  space that is 0.01  $\mathcal{R}$  in width). Given that actual values for  $R_g$  and  $R_e$  mean little (since one rarely deals with polyglycines of length 10), actual values are omitted.  $\chi$  ranges from -1 to +1.

87 As evident in Fig. 3, the distributions within the Ramachandran plot are faithfully reflected in corre-  
 88 sponding distributions within Ramachandran number space. This paper shows how the Ramachandran  
 89 number is both compact enough and informative enough to generate immediately useful graphs (multi-  
 90 angle pictures or MAPs) of a dynamic protein backbone.

## 91 REASON TO USE THE RAMACHANDRAN NUMBER

### 92 Ramachandran numbers are structurally meaningful

93 In addition to resolving positions of secondary structures (Fig. 3),  $\mathcal{R}$  relates well to structural measures  
 94 such as radius of gyration ( $R_g$ ), end-to-end distance ( $R_e$ ) and chirality ( $\chi$ ). These relationships are  
 95 shown in Fig. 4. Note that chirality comes in many forms, e.g., one could be talking about different  
 96 stereo-isomers, such as L vs D amino acids, or one could be concerned with left-twisting versus  
 97 right-twisting backbones, i.e., handedness Mannige (2017). This report will primarily be focused  
 98 on chirality in context of backbone twist/handedness.

99 The trends in Fig. 4 show that as one progresses from low to high  $\mathcal{R}$ , various structural proper-  
 100 ties also progress smoothly. Additionally, backbones that display similar  $\mathcal{R}$  also show little varia-  
 101 tion in structural properties, as evidenced by the small standard deviation bars. It is also important  
 102 to note that the standard deviations shown in Fig. 4 were calculated by first populating every possi-  
 103 ble region of  $(\phi, \psi)$ -space. However, in reality, most regions of  $(\phi, \psi)$ -space are unoccupied due  
 104 to steric/electrostatic constraints, which means that these error bars are likely to be even smaller  
 105 than depicted. Finally, the  $\mathcal{R}$  number is calculated by taking ‘sweeps’ of the  $(\phi, \psi)$ -space in lines  
 106 that are parallel to the negatively-sloping diagonal. Interestingly, such ‘sweeps’ encounter only one  
 107 major (dense) region within  $(\phi, \psi)$ -space (e.g.,  $\mathcal{R}$ ’s in the general vicinity of 0.34 represent struc-  
 108 tures that resemble  $\alpha$  helices. This means that  $\mathcal{R}$  can also be used to assess the types of secondary  
 109 structure present in a protein conformation.

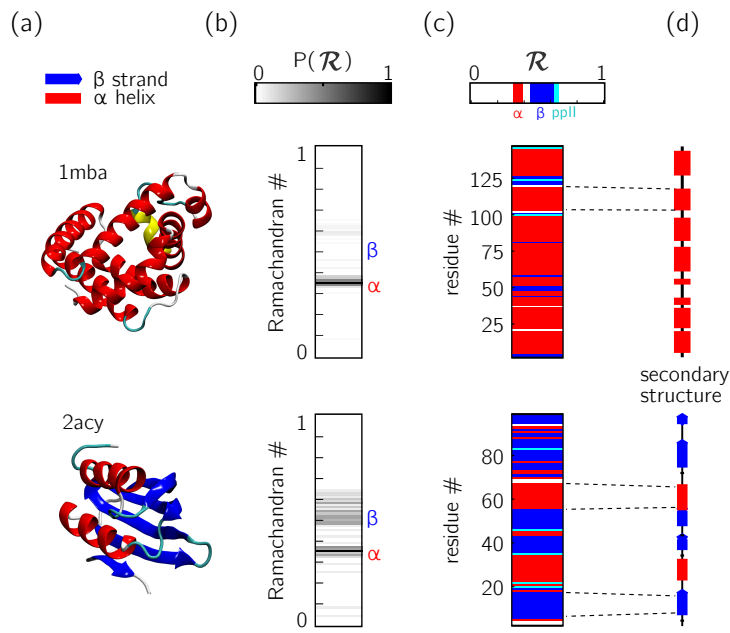


**Figure 5. Two types of  $\mathcal{R}$ -codes.** Digesting protein structures (a) using  $\mathcal{R}$  numbers either as histograms (b) or per-residue codes (c) allow for compact representations of salient structural features. For example, a single glance at the histograms indicate that protein **1mba** is likely all  $\alpha$ -helical, while **2acy** is likely a mix of  $\alpha$ -helices and  $\beta$ -sheets. Additionally, residue-specific codes (c) not only indicate secondary structure content, but also exact **secondary** structure stretches (compare to d), which gives a more complete picture of how the protein is linearly arranged.

### 110 Ramachandran codes are stackable

111 **An important aspect of the Ramachandran number ( $\mathcal{R}$ ) lies in its compactness compared to the**  
 112 **traditional Ramachandran pair ( $\phi, \psi$ ). The value of the conversion from ( $\phi, \psi$ )-space to  $\mathcal{R}$ -space**  
 113 **is that the structure of a protein can be described in various one-dimensional arrays (per-structure**  
 114 **“Ramachandran codes” or “ $\mathcal{R}$ -codes” or multi-angle maps); see, e.g., Fig. 5.**

115 In addition to assuming a small form factor,  $\mathcal{R}$ -codes may then be *stacked* side-by-side for visual and  
 116 computational analysis. There lies its true power.

117 For example, the one- $\mathcal{R}$ -to-one-residue mapping means that the entire residue-by-residue structure  
 118 of a protein can be shown using a string of  $\mathcal{R}_i$ s (which would show regions of secondary structure and  
 119 disorder, for starters). Additionally, an entire protein’s backbone makeup can be shown as a histogram in  
 120  $\mathcal{R}$ -space (which may reveal a protein’s topology). The power of this format lies not only in the capacity  
 121 to distill complex structure into compact spaces, but in its capacity to display *many* complex structures in  
 122 this format, side-by-side (stacking).

123 Peptoid nanosheets (Mannige *et al.*, 2015) will be used here as an example of how multiple structures,  
 124 in the form of  $\mathcal{R}$ -codes, may be stacked to provide immediately useful pictograms. **Peptoids are stereo-**  
 125 **isomers of peptides, where the sidechain is attached to the backbone nitrogen rather than the  $\alpha$**   
 126 **carbon atom. Since both peptoids and peptides share identical backbone connectivity, the analysis**  
 127 **described below could be applied to both peptides and peptoids.**

128 Peptoid nanosheets are a recently discovered peptide-mimic that, in one molecular dynamics simula-  
 129 tion (Mannige *et al.*, 2015), were shown to display a novel secondary structure. In the reported model  
 130 (Mannige *et al.*, 2015), each peptoid within the nanosheet displays backbone conformations that alternate  
 131 in chirality, causing the backbone to look like a meandering snake that nonetheless maintains an overall  
 132 linear direction. This secondary structure was discovered by first setting up a nanosheet where all peptoid  
 133 backbones were restrained to be fully extended (Fig. 6a, left), after which the restraints were energetically  
 134 softened (a, middle) and completely **released** (a, right). As evident in Fig. 6b and Fig. 6c, the two types of  
 135  $\mathcal{R}$ -code stacks display salient information at first glance: 1) Fig. 6b shows that the extended backbone first  
 136 undergoes some rearrangement with softer restraints, and then becomes much more binary in arrangement

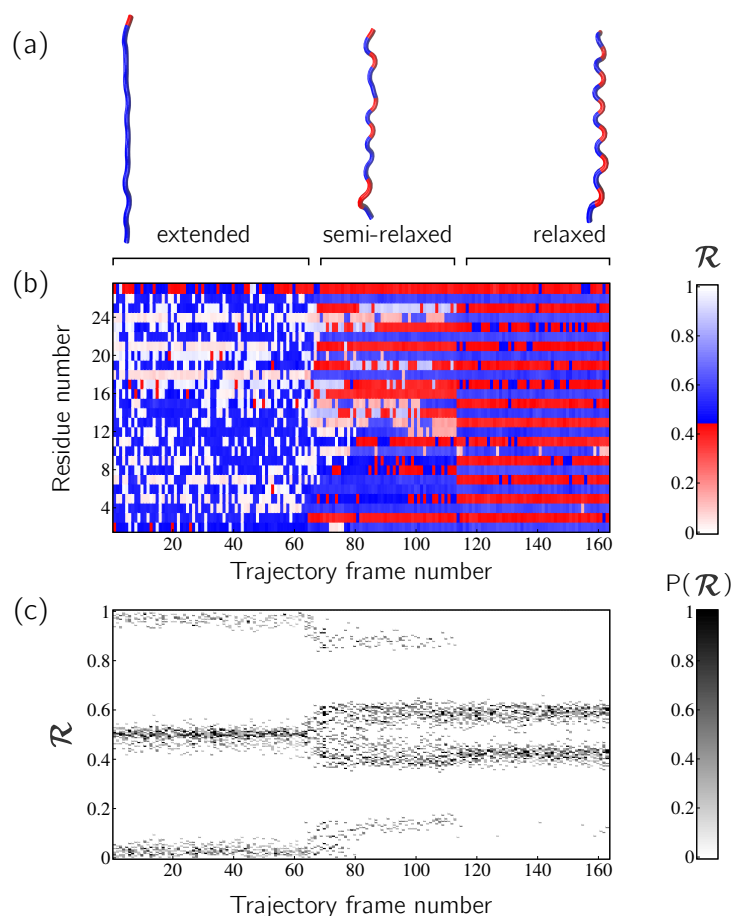


**Figure 6. Stacked  $\mathcal{R}$ -codes provide useful information at a glance. Each panel represents a molecular dynamics simulation of a peptoid nanosheet (Mannige *et al.*, 2016), where each peptoid backbone was held (energetically restrained) in extended state in the beginning, upon which each backbone was allowed to relax by lifting the restrains. Panel (a) displays representative structures from each stage of the simulation. Panel (b) represents how the per-residue structure of the peptide evolved over ‘time’ (the progression of time is represented as increasing frame number). Panel (c) represents how the general distribution of backbone conformations in the peptoid (as evident by the  $\mathcal{R}$  histogram) evolves over time.**

137 as we look down the backbone (excepting the low-order region in the middle, unshown in Fig. 6a); and  
 138 2) Fig. 6c shows that lifting restraints on the backbone causes a dramatic change in backbone topology,  
 139 namely a birth of a bimodal distribution evident in the two parallel horizontal bands.

140 By utilizing  $\mathcal{R}$ , maps such as those in Fig. 6 provide information about every  $\phi$  and  $\psi$  within the  
 141 backbone. As such, these maps are dubbed MAPs, for Multi Angle Pictures. A Python package called  
 142 BACKMAP created Fig. 6a and b, which is provided as a GitHub repository at <https://github.com/ranjanmannige/BackMAP>. BACKMAP takes in a PDB structure file containing a single  
 143 structure, or multiple structures separated by the code ‘MODEL’.  
 144

#### 145 **Case study: picking out subtle differences from high volume of data**

146 This section expands on the notion that  $\mathcal{R}$ -numbers – due to their compactness/stackability – can be used  
 147 to pick out backbone structural trends that would be hard to decipher using any other metric. For example,  
 148 it is well known that prolines (P) display unusual backbone behavior: in particular, proline backbones  
 149 occupy structures that are close to but distinct from  $\alpha$ -helical regions. Due to the two-dimensionality  
 150 of Ramachandran plots (Fig. 7a), such distinctions are hard to visually pick out from Ramachandran  
 151 plots. However, stacking per-amino-acid  $\mathcal{R}$ -codes side by side make such differences patent (Fig. 7b; see  
 152 arrow).

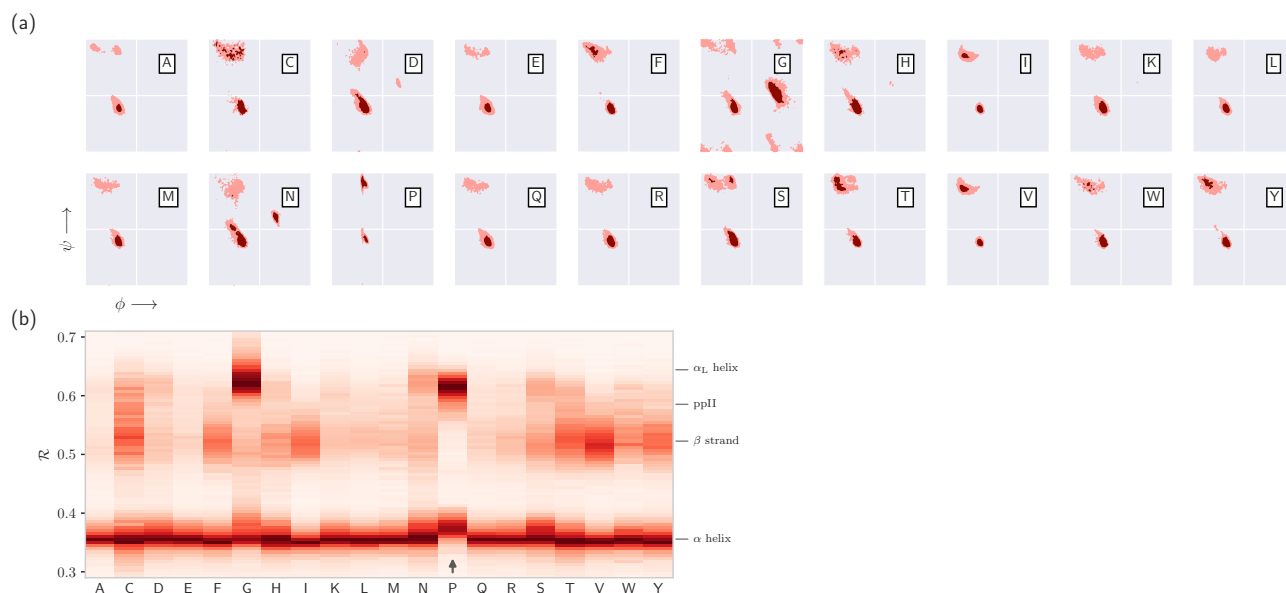


**Figure 7. Combining Ramachandran plots for all amino acids into one graph.** Panel (a) shows the per-amino acid backbone behavior of an average protein found in the protein databank (PDB). While these plots are useful, it is difficult to compare such plots. For example, it is hard to pick out the change in the  $\alpha$ -helical region of the proline plot (P). However, when we convert Ramachandran plots to Ramachandran lines [by converting  $(\phi_i, \psi_i) \rightarrow \mathcal{R}_i$ ], we are able to conveniently “stack” Ramachandran lines calculated for each residue. Then, even visually, it is obvious that proline does not occupy the canonical  $\alpha$ -helical region, which is not evident to an untrained eye in (a).

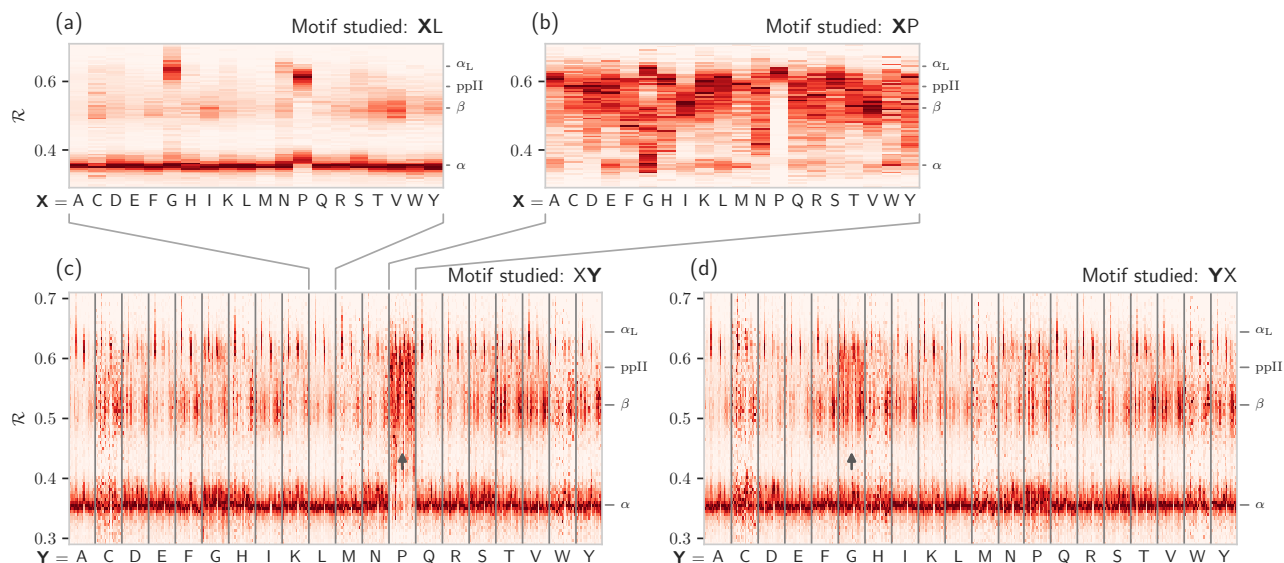


**Figure 8. How residue neighbors modifies structure.** Similar to Fig. 7b, Panel (a) represents the behavior of an amino acid ‘X’ situated *before* a leucine (XL; assuming that we are reading a sequence from the N terminal to the C terminal). Panel (b) similarly represents the behavior of specific amino acids situated before a proline (XP). While residues preceding a leucine behave similarly to their average behavior (Fig. 7a), most residues preceding prolines appear to be enriched in structures that change ‘direction’ or backbone chirality (this is evident by many amino acids switching from  $\mathcal{R} < 0.5$  to  $\mathcal{R} > 0.5$ ). Panels (c) and (d) show the behavior of individual amino acids when situated before and after each of the 20 amino acids, respectively. Panels (c) and (d) show a major benefit of side-by-side Ramachandran line “stacking”: general trends become much more obvious. For example, it is evident that prolines dramatically modify the structure of an amino acid preceding it (compared to average behavior of amino acids in Fig. 7b), while residues following glycines also have a higher prevalence of  $\mathcal{R} > 0.5$  conformations (both trends are indicated by small arrows). Such trends, while previously discovered (see text), would not be accessible when naively considering Ramachandran plots because one would require 400 ( $20 \times 20$ ) distinct Ramachandran plots to compare. Note that the statistics for each  $\mathcal{R}$ -line in (c) and (d) are dependent on the joint prevalence of the residues being considered. For this reason, some  $\mathcal{R}$ -lines (e.g., those 7/17 associated with cysteines) look more rough or ‘dotty’ than others..

153 It is also known that amino acids preceding prolines display unusual shift in backbone twist/chirality.  
 154 For example, Fig. 8c shows that amino acids appearing before prolines behave differently than they  
 155 would otherwise (see the upward-facing arrow). Additionally, amino acids following glycines also  
 156 appear to have their structures modified (Fig. 8d; upward arrow). Note that these results are  
 157 not new, and it has already been confirmed that, e.g., nearest neighbors affect the conformational  
 158 behavior of an amino acid as witnessed within Ramachandran plots (Ting *et al.*, 2010), and proline  
 159 changes the backbone conformation of the preceding residue (Gunasekaran *et al.*, 1998; Ho and  
 160 Brasseur, 2005). However, Figs. 7 and 8 indicate that such information can be more concisely  
 161 shown/identified when structures are stacked side-by-side in the form of  $\mathcal{R}$ -codes. Such subtle  
 162 changes are often witnessed when protein backbones transition from one state to another.

## 163 USING THE BACKMAP PYTHON MODULE

### 164 Installation

165 BACKMAP may either be installed locally by downloading the [GitHub repository](#), or installed directly  
 166 by running the following line in the command prompt (assuming that pip exists): > pip install  
 167 backmap

### 168 Usage

169 The module can either be imported and used within existing scripts, or used as a standalone package using  
 170 the command 'python -m backmap'. First the in-script usage will be discussed.

#### 171 In-script usage I: first simple test

172 The simplest test would be to generate Ramachandran numbers from  $(\phi, \psi)$  pairs:

---

```
173 # Import module
174 import backmap
175 # Convert (phi, psi) to R
176 print backmap.R(phi=0, psi=0) # Expected output: 0.5
177 print backmap.R(phi=-180, psi=-180) # Expected output: 0.0
178 print backmap.R(phi=180, psi=180) # Expected output: 1.0 (equivalent in meaning to 0)
```

---

#### 181 In-script usage II: basic usage for creating Multi-Angle Pictures (MAPs)

182 The following code shows how Multi-Angle Pictures (MAPs) of protein backbones can be generated:

##### 183 1. Select and read a protein PDB structure

184 Each trajectory frame must be a set of legitimate protein databank "ATOM" records separated by  
 185 "MODEL" keywords (distinct models show up as distinct frames on the x-axis or abscissa).

---

```
186 import backmap
187 pdbfn = './pdb/nanosheet_birth_U7.pdb' # Set pdb name
188 data = backmap.read_pdb(pdbfn) # READ PDB in the form of a matrix with columns
```

---

191 Here, 'data' is a 2d array with four columns ['model', 'chain', 'resid', 'R']. The first row of  
 192 'data' is the header (i.e., the name of the column, e.g., 'model'), with values that follow.

##### 193 2. Select color scheme (color map)

194 In addition to custom colormaps listed in the next section, one can also use **traditionally** available  
 195 colormaps at [matplotlib.org](http://matplotlib.org) (e.g., 'Reds' or 'Reds\_r').

---

```
196 # setting the name of the colormap
197 cmap = "SecondaryStructure"
```

---

##### 200 3. Draw per-chain MAPs

---

```
201 # Grouping by chain
202 grouped_data = backmap.group_by(data, group_by='chain',
203                                columns_to_return=['model', 'resid', 'R'])
204 for chain in grouped_data.keys(): # Going through each chain
205     # Getting the X,Y,Z values for each entry
206     models, residues, Rs = grouped_data[chain]
```

---

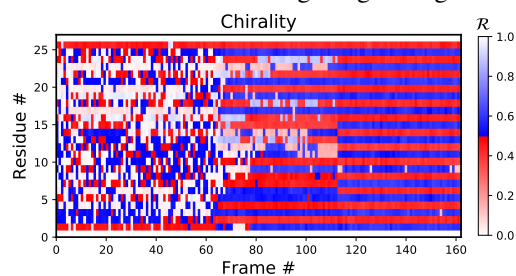
```

208 # Finally, creating (but not showing) the graph 12
209 backmap.draw_xyz(X = models , Y = residues , Z = Rs 13
210 , xlabel = 'Frame #' , ylabel = "Residue #" , zlabel = '\mathcal{R}$' 14
211 , cmap = cmap , title = "Chain: '"+chain+"' " 15
212 , vmin=0, vmax=1) 16
213 # Now, we display the graph: 17
214 plt.show() # ... one can also use plt.savefig() to save to file 18

```

---

216 Running the module as a standalone script would produce all these graphs automatically. 'plt.show()' 217 would result in the following image being rendered:



218

219 Additionally, by changing how one assigns values to 'X' and 'Y', one can easily construct and draw 220 other types of graphs such as time-resolved histograms, **per-residue fluctuations when compared 221 to the first ( $D_1$ ) and previous structure ( $D_{-1}$ ) within the trajectory**, etc.

### 222 In-script usage III: Creating custom graphs

223 Other types of **graphs** can be easily created by modifying part three of the code above. For example, the 224 following code creates histograms of R, one for each model (starting from line 9 above).

```

225 

---

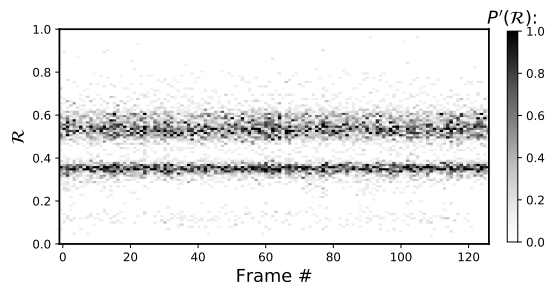

226 for chain in grouped_data.keys(): 9
227     models, residues, Rs = grouped_data[chain] 10
228 11
229     'Begin custom code' 12
230     X = []; Y=[]; Z=[]; # Will set X=model, Y=R, Z=P(R) 13
231     # Bundling the three lists into one 2d array 14
232     new_data = np.array(zip(models, residues, Rs)) 15
233     # Getting all R values, model by model 16
234     for m in sorted(set(new_data[:,0])): # column 0 is the model column 17
235         # Getting all Rs for that model # 18
236         current_rs = new_data[np.where(new_data[:,0]==m)][:,2] # column 2 contains R 19
237         # Getting the histogram 20
238         a,b = np.histogram(current_rs, bins=np.arange(0,1.01,0.01)) 21
239         max_count = float(np.max(a)) 22
240         for i in range(len(a)): 23
241             X.append(m); Y.append((b[i]+b[i+1])/2.0); Z.append(a[i]/float(np.sum(a))); 24
242         'End custom code' 25
243 26
244     # Finally, creating (but not showing) the graph 27
245     draw_xyz(X = X , Y = Y , Z = Z 28
246             , xlabel = 'Frame #' , ylabel = "\mathcal{R}$" , zlabel = "$P'(\mathcal{R})$" 29
247             , cmap = 'Greys' , ylim=[0,1]) 30
248     plt.yticks(np.arange(0,1.00001,0.2)) 31
249     # Now, we display the graph: 32
250     plt.show() # ... one can also use plt.savefig() to save to file 33
251 

---



```

252 The code above results in the following graph:



253

#### 254 In-script usage IV: Available color schemes (CMAPs)

255 Aside from the general color maps (cmaps) that exist in matplotlib (e.g., ‘Greys’, ‘Reds’, or, god forbid,  
 256 ‘jet’), BACKMAP provides two new colormaps: ‘Chirality’ (key: +-twists – red; –ve twists: blue),  
 257 and ‘SecondaryStructure’ (key: *potential* helices – red; sheets – blue; ppII helices – cyan). right  
 258 twisting backbones are shown in red; left twisting backbones are shown in blue). Fig. 9 shows how  
 259 a single protein ensemble may be described using these schematics. As illustrated in Fig. 9b, cmap  
 260 available within the standard matplotlib package do not distinguish between major secondary structures  
 261 well, while those provided by BACKMAP do. In case it is known that the protein backbone accesses  
 262 non-traditional regions of the Ramachandran plot, a four-color schematic will be needed (see below for  
 263 more discussions).

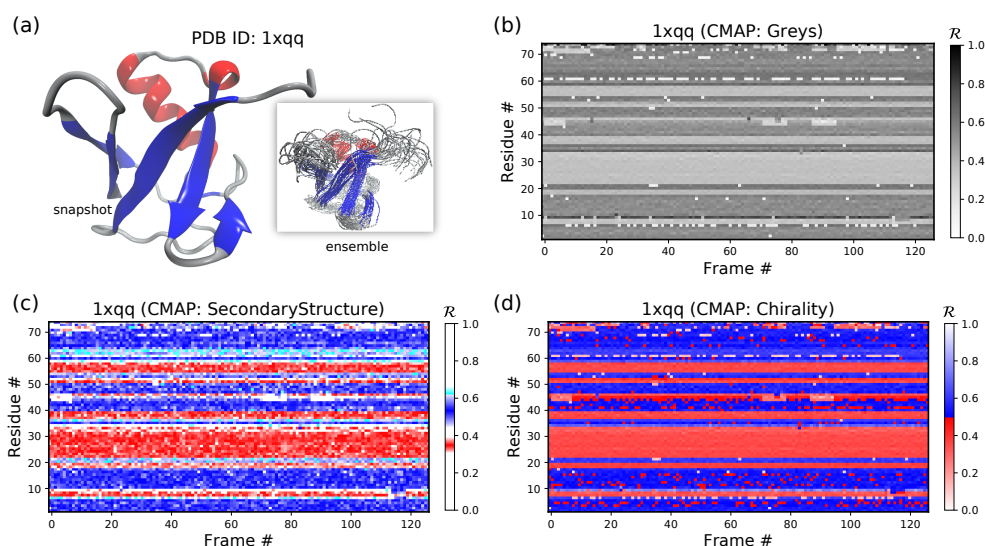


**Figure 9.** A protein ensemble (a) along with some MAPs colored with different themes (b-d). Panels (c) and (d) are provided by the BACKMAP module. In Panel (c),  $\beta$ -sheets are shown in blue and all helices are shown in red. In Panel (d), right-handed and left-handed backbone twists are shown as red and blue respectively.

#### 264 Stand Alone Usage

265 BACKMAP can be used as a stand alone package by running ‘> python -m backmap -pdb <pdb\_dir\_or\_file>’.  
 266 The sections below describes the expected outputs and how they may be interpreted.

#### 267 Stand Alone Example I: A Stable Protein

268 Panels (b) through (f) of Fig. 10 below were created by running ‘> python -m backmap ./tests/pdbs/1xqq.pdb’  
 269 (Panel (a) was created using VMD). These graphs indicate that protein 1xqq describes a conformationally  
 270 stable protein, since each residue fluctuates little in color (structure) over ‘time’ (c,d; here and below, it is  
 271 assumed that discrete models represent distinct states of the protein over ‘time’), show little change in the  
 272  $\mathcal{R}$  histogram over time (b) and show few enduring fluctuations (e,f; see Methods).

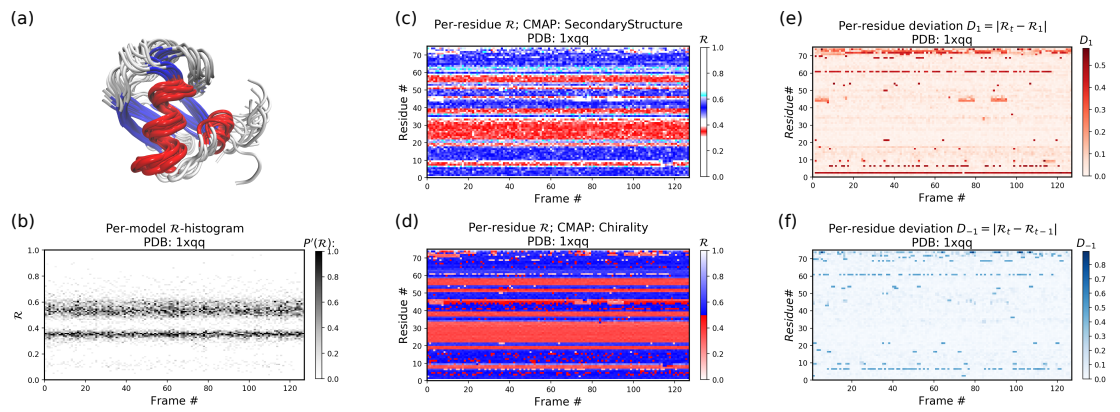


**Figure 10.** Protein **1xqq** describes a stable protein. **Panel (a)** represents the entire ensemble, **Panel(b)** represents a histogram distribution of  $\mathcal{R}$ , **Panels (c) and (d)** represent two ways color per-residue  $\mathcal{R}$  plots, and **Panels (e) and (f)** are two ways to describe backbone fluctuation over time.

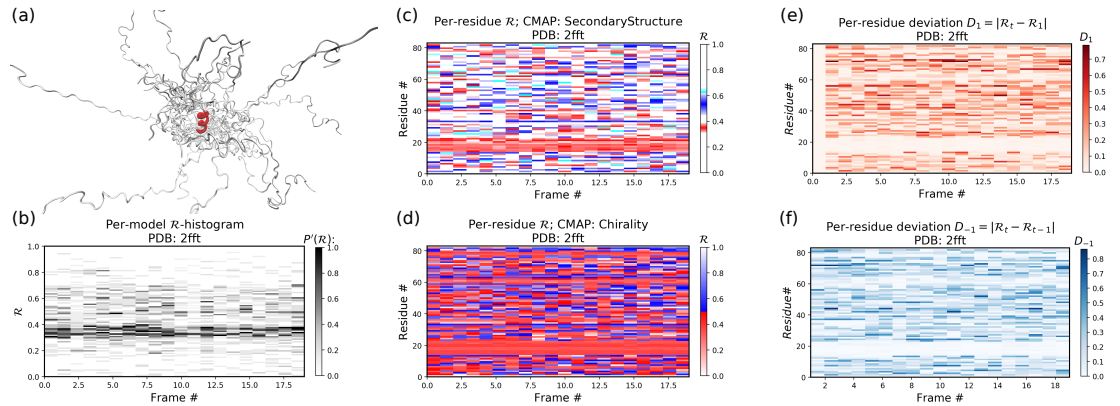


**Figure 11.** Protein **2fft** describes an intrinsically disordered protein, with one stable helix in red. **Descriptions of each panel are identical to that of Fig. 10.**

273 In particular, each column in Panel (b) describes the histogram in Ramachandran number ( $\mathcal{R}$ ) space  
 274 for a single model/timeframe. These histograms show the presence of both  $\alpha$ -helices (at  $\mathcal{R} \approx 0.34$ )  
 275 and  $\beta$ -sheets (at  $\mathcal{R} \approx 0.52$ ). Additionally, Panels (c) and (d) describe per-residue conformational plots  
 276 (colored by two different metrics or CMAPs), which show that most of the protein backbone remains  
 277 relatively stable over time (e.g., few fluctuations in state or ‘color’ are evident over frame #). Finally,  
 278 Panel (e) describes the extent towards which a single residue’s state has deviated from the first frame,  
 279 and Panel (f) describes the extent towards which a single residue’s state has deviated from its state in the  
 280 previous frame. All these graphs, show that this protein is relatively conformationally stable.

### 281 Stand Alone Example II: An Intrinsically Disordered Protein

282 Fig. 11 is identical to Fig. 10, except that the panels pertain to an intrinsically disordered protein **2fft**  
 283 whose structural ensemble describes dramatically distinct conformations.

284 As compared to the conformationally stable protein above, protein **2fft** is much more flexible. Panel  
 285 (b) shows that the states accessed per model are diverse and dramatically fluctuate over the entire range of  
 286  $\mathcal{R}$  (this is especially true when compared to a stable protein, see Fig. 10b).

287 The diverse states occupied by each residue (Panels (c) and (d)) confirm the conformational variation  
 288 displayed by most of the backbone (Panels (e) and (f)) similarly show how most of the residues fluctuate  
 289 dramatically).

290 Yet, interestingly, Panels (c) through (f) also show an **unusually** stable region – residues 15 through  
 291 25 – which consistently display the same conformational ( $\alpha$ -helical) state at  $\mathcal{R} \approx 0.34$  (interpreted as the  
 292 color red in Panel (c)). This trend would be hard to recognize by simply looking at the structural ensemble

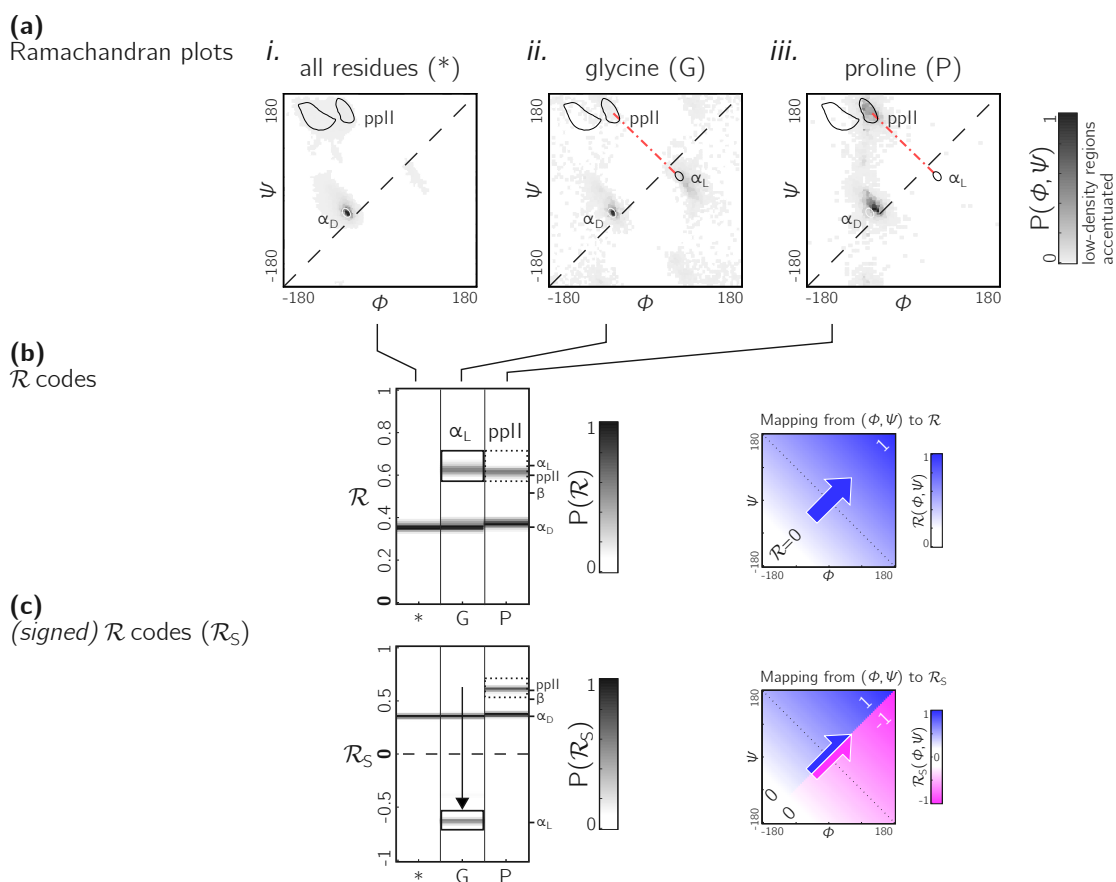


**Figure 12. Signed  $\mathcal{R}$ s are required for non-chiral backbones.** While the backbones of most amino acids occupy the top of the positively sloped diagonal (dashed in b), non chiral amino acids such as Glycines (or their N-substituted variants – peptoids) display no such preference, which causes distinct secondary structures that lie on the same ‘sweep’ to be localized at similar regions in  $\mathcal{R}$  (e.g., in b, polyproline-II and  $\alpha_D$  helices both localize at  $\mathcal{R} \approx 0.6$ ). However, a signed Ramachandran number ( $\mathcal{R}_S$ ) solves this overlap by multiplying those  $\mathcal{R}$ ’s derived from backbones with  $\phi > \psi$  by  $-1$ . The resolving power of  $\mathcal{R}_S$  is evident by the separation of polyproline-II and  $\alpha_D$  helices (c). The mapping of  $(\phi, \psi)$  to  $\mathcal{R}$  and  $\mathcal{R}_S$  are shown to the right of each respective  $\mathcal{R}$ -plot (b,c).

293 (Panel (a)).

### 294 A signed Ramachandran number for ‘misbehaving’ backbones

295 The Ramachandran number increases in value from the bottom left of the Ramachandran plot to the  
 296 top right in sweeps that are parallel to the negative sloping diagonal. As discussed in Mannige *et al.*  
 297 (2016), this method of mapping a two-dimensional space into one number is still structurally meaningful  
 298 and descriptive because 1) most structural features of the protein backbone – e.g. radius of gyration  
 299 (Mannige *et al.*, 2016), end-to-end distance (Mannige *et al.*, 2016), and chirality (Mannige, 2017) – vary  
 300 little along lines parallel to the negatively-sloping diagonal (this is indicated by relatively small standard  
 301 deviations in structural metrics for similar  $\mathcal{R}$ s; Fig. 4), and 2) most protein backbones display chiral  
 302 centers and therefore predominantly appear on the top left region of the Ramachandran plot (above the  
 303 dashed diagonal in Fig. 12a-(i)).

304 However, not all backbones localize in only one half of the Ramachandran plot. Particularly, among  
 305 biologically relevant amino acids, glycine occupies both regions of the Ramachandran plot (Fig. 12a-(ii);  
 306 of note, the  $\alpha_L$  helix region becomes relatively prominent). On the other hand, prolines are known to form  
 307 polyproline-II helices (ppII in Fig. 12a-(iii)), which falls on almost the same ‘sweep’ as glycine rich pep-  
 308 tides (red dot-dashed line). In situations where both prolines and glycines are abundant, the Ramachandran  
 309 number ( $\mathcal{R}$ ) would fail to distinguish  $\alpha_L$  from ppII (Fig. 12b; regions outlined by rectangles).

To accommodate the situation where achiral backbones are expected (eg., if peptoids or polyglycines are being studied), an additional Ramachandran number – the *signed* Ramachandran number  $\mathcal{R}_S$  – is introduced here.  $\mathcal{R}_S$  is identical to the original number in magnitude, but which changes sign from + to – as you approach  $\mathcal{R}$  numbers that are to the right (or below) the positively sloped diagonal. I.e.,

$$\mathcal{R}_S = \begin{cases} \mathcal{R} & , \text{ if } \psi \geq \phi \\ \mathcal{R} \times -1 & , \text{ if } \psi < \phi \end{cases} \quad (3)$$

310 As an example of the utility of  $\mathcal{R}_S$ , Fig. 12c shows that  $\mathcal{R}_S$  easily distinguishes  $\alpha_D$  from ppII.

311 Note that the signed  $\mathcal{R}_S$ , while useful, would be important in very limited scenarios, as more than  
312 96% of the amino acids in the Protein Databank (PDB) occupy the upper-left region of the Ramachandran  
313 plot (with the 3% of ‘rule breakers’ contributed mostly by glycines).

## 314 CONCLUSION

315 A simpler Ramachandran number is reported –  $\mathcal{R} = (\phi + \psi + 2\pi)/(4\pi)$  – which, while being a single  
316 number, provides much information. For example, as discussed in Mannige *et al.* (2016),  $\mathcal{R}$  values  
317 above 0.5 are left-handed **in twist**, while those below 0.5 are right handed,  $\mathcal{R}$  values close to 0, 0.5 and  
318 1 are extended,  $\beta$ -sheets occupy  $\mathcal{R}$  values at around 0.52, right-handed  $\alpha$ -helices hover around 0.34.  
319 Given the Ramachandran number’s ‘stackability’, single graphs can hold detailed information of the  
320 progression/evolution of molecular trajectories. Indeed, Fig. 8 shows how 400 distinct Ramachandran  
321 plots can easily be fit into one graph when using  $\mathcal{R}$ . Finally, a python script/module (BACKMAP) has  
322 been provided in an online [GitHub repository](#) to promote the utility of  $\mathcal{R}$  as a universal metric.

## 323 MATERIALS

324 Statistics about single amino acid conformations and secondary structures (excepting polyproline II  
325 helices) were derived from the Structural Classification of Proteins or SCOPe website [Release 2.06; Fox  
326 *et al.* (2014)]. This database, currently available at [http://scop.berkeley.edu/downloads/  
327 pdbstyle/pdbstyle-sel-gs-bib-40-2.06.tgz](http://scop.berkeley.edu/downloads/pdbstyle/pdbstyle-sel-gs-bib-40-2.06.tgz), contains 13,760 three-dimensional protein  
328 conformations (one domain per conformation) with lower than 40% sequence identity. Secondary structure  
329 annotations were assigned using the DSSP algorithm (Kabsch and Sander, 1983), although the STRIDE  
330 algorithm (Frishman and Argos, 1995) provides qualitatively identical distributions. **These statistics  
331 were used to produce distributions within Fig. 2a and Fig. 3a,c.**

332 Given the absence of polyproline II helix (ppII) annotation in the present version of DSSP, statistics for  
333 polyproline II helices (**used to generate the ppII distributions in Fig. 2a and Fig. 3a,c**) were obtained  
334 from segments within 16,535 proteins annotated by PolyprOnline (Chebrek *et al.*, 2014) to contain three  
335 or more residues of the secondary structure.

336 **Fig. 6** represents a trajectory of a portion of a single peptoid backbone within a ‘relaxing’ peptoid  
337 nanosheet bilayer. The conformation of this backbone – derived from work by Mannige *et al.* (2015) and  
338 Mannige *et al.* (2016) – is also available as ‘tests/pdbs/nanosheet\_birth\_U7.pdb’ within the companion  
339 [GitHub repository](#).

340 The following protein structures were obtained from the Protein DataBank (PDB): *1mba*, *2acy*, *1xqq*,  
341 and *2fft*. The first two in the list (*1mba*, *2acy*) describe single conformations and the last two (*1xqq*,  
342 *2fft*) describe ensembles.  **$\mathcal{R}$ -based multi-angle pictures (MAPs) were created for each structure  
343  $X \in [\textit{nanosheet\_birth\_U7.pdb}, \textit{2fft}, \textit{2acy}, \textit{1xqq}, \textit{1mba}]$  using the following command line code:**

344 **> python -m backmap -pdb tests/pdbs/*X*.pdb**

345 **The output of this command line implementation were used in panels (b) onwards of Figs. 5, 6, 9,  
346 10 and 11.**

**In order to describe change in structural, this report uses two metrics for structural deviation:  
deviation in structure when compared to the first conformation in the trajectory ( $D_1$ ), and the pre-  
vious conformation in the trajectory ( $D_{-1}$ ). For any residue  $r$  at time  $t$ , these equations can be  
described as follows:**

$$D_1 = |\mathcal{R}_t - \mathcal{R}_1|, \quad D_{-1} = |\mathcal{R}_t - \mathcal{R}_{t-1}|. \quad (4)$$

347 All three-dimensional representations of proteins (Panel (a) in Figs. 5, 6, 9, 10 and 11) were  
 348 created using VMD (Humphrey *et al.*, 1996). Finally, all other figures – excepting Fig. 1 that is de-  
 349 rived from Mannige *et al.* (2016) – were created using helper Python scripts available in manuscrip-  
 350 t/python\_generators/ within the companion GitHub repository.

## 351 ACKNOWLEDGMENTS

352 During the development of this paper, RVM was partially supported by the Defense Threat Reduction  
 353 Agency under contract no. IACRO-B0845281. RVM thanks Alana Canfield Mannige for her critique. The  
 354 notion of the signed Ramachandran number emerged from discussions with Joyjit Kundu and Stephen  
 355 Whitelam while at the Molecular Foundry at Lawrence Berkeley National Laboratory (LBNL). This work  
 356 was partially done at the Molecular Foundry at LBNL, supported by the Office of Science, Office of Basic  
 357 Energy Sciences, of the U.S. Department of Energy under Contract No. DE-AC02-05CH11231.

## 358 APPENDIX

### 359 Simplifying the Ramachandran number ( $\mathcal{R}$ )

360 This section will derive the simplified Ramachandran number presented in this paper from the more  
 361 complicated looking Ramachandran number introduced previously (Mannige *et al.*, 2016).

Assuming the bounds  $\phi \in [\phi_{\min}, \phi_{\max})$  and  $\psi \in [\psi_{\min}, \psi_{\max})$ , the previously described Ramachandran number takes the form

$$\mathcal{R}(\phi, \psi) \equiv \frac{R_{\mathbb{Z}}(\phi, \psi) - R_{\mathbb{Z}}(\phi_{\min}, \phi_{\min})}{R_{\mathbb{Z}}(\phi_{\max}, \phi_{\max}) - R_{\mathbb{Z}}(\phi_{\min}, \phi_{\min})}, \quad (5)$$

where,  $\mathcal{R}(\phi, \psi)$  is the Ramachandran number with range  $[0, 1)$ , and  $R_{\mathbb{Z}}(\phi, \psi)$  is the *unnormalized* integer-spaced Ramachandran number whose closed form is

$$R_{\mathbb{Z}}(\phi, \psi) = \left\lfloor (\phi - \psi + \lambda)\sigma/\sqrt{2} \right\rfloor + \left\lfloor \sqrt{2}\lambda\sigma \right\rfloor \left\lfloor (\phi + \psi + \lambda)\sigma/\sqrt{2} \right\rfloor. \quad (6)$$

362 Here,  $\lfloor x \rfloor$  rounds  $x$  to the closest integer value,  $\sigma$  is a scaling factor, discussed below, and  $\lambda$  is the  
 363 range of an angle in degrees (i.e.,  $\lambda = \phi_{\max} - \phi_{\min}$ ). Effectively, this equation does the following. **1)** It  
 364 divides up the Ramachandran plot into  $(360^\circ \sigma^{1/2})^2$  squares, where  $\sigma$  is a user-selected scaling factor  
 365 that is measured in reciprocal degrees [see Fig. 8b in Mannige *et al.* (2016)]. **2)** It then assigns integer  
 366 values to each square by setting the lowest integer value to the bottom left of the Ramachandran plot  
 367 ( $\phi = -180^\circ, \psi = -180^\circ$ ) and proceeding from the bottom left to the top right by iteratively slicing down  
 368  $-1/2$  sloped lines and assigning increasing integer values to each square that one encounters. **3)** Finally,  
 369 the equation assigns any  $(\phi, \psi)$  pair within  $\phi, \psi \in [-\phi_{\min}, \phi_{\max})$  to the integer value ( $R_{\mathbb{Z}}$ ) assigned to the  
 370 divided-up square that they exist in.

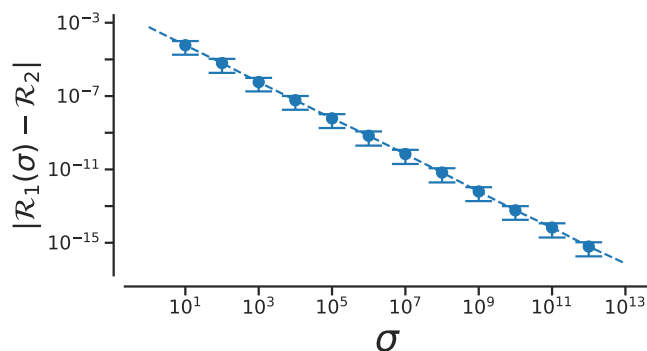


**Figure 13.** The increase in the accuracy measure ( $\sigma$ ) for the original Ramachandran number (Eqn. 6) results in values that tend towards the new Ramachandran number proposed in this paper (Eqn. 2).

Combining the two equations (Eqns. 5 and 6) results in the following, rather imposing, equation for the Ramachandran number:

$$\mathcal{R}(\phi, \psi) = \frac{\left( \begin{array}{cc} \left\lfloor (\phi - \psi + \lambda)\sigma/\sqrt{2} \right\rfloor & + \left\lfloor \sqrt{2}\lambda\sigma \right\rfloor \left\lfloor (\phi + \psi + \lambda)\sigma/\sqrt{2} \right\rfloor \\ - \left\lfloor (\phi_{\min} - \psi_{\min} + \lambda)\sigma/\sqrt{2} \right\rfloor & - \left\lfloor \sqrt{2}\lambda\sigma \right\rfloor \left\lfloor (\phi_{\min} + \psi_{\min} + \lambda)\sigma/\sqrt{2} \right\rfloor \end{array} \right)}{\left( \begin{array}{cc} \left\lfloor (\phi_{\max} - \psi_{\max} + \lambda)\sigma/\sqrt{2} \right\rfloor & + \left\lfloor \sqrt{2}\lambda\sigma \right\rfloor \left\lfloor (\phi_{\max} + \psi_{\max} + \lambda)\sigma/\sqrt{2} \right\rfloor \\ - \left\lfloor (\phi_{\min} - \psi_{\min} + \lambda)\sigma/\sqrt{2} \right\rfloor & - \left\lfloor \sqrt{2}\lambda\sigma \right\rfloor \left\lfloor (\phi_{\min} + \psi_{\min} + \lambda)\sigma/\sqrt{2} \right\rfloor \end{array} \right)} \quad (7)$$

However useful Eqn. 7 is, the complexity of the equation may be a deterrent towards utilizing it. This paper reports a simpler equation that is derived by taking the limit of Eqn. 7 as  $\sigma$  tends towards  $\infty$ . In particular, when  $\sigma \rightarrow \infty$ , Eqn. 7 becomes

$$\mathcal{R}(\phi, \psi) = \lim_{\sigma \rightarrow \infty} \bar{\mathcal{R}}(\phi, \psi) = \frac{\phi + \psi - (\psi_{\min} + \psi_{\min})}{(\phi_{\max} + \psi_{\max}) - (\phi_{\min} + \psi_{\min})}. \quad (8)$$

371 Assuming that  $\phi, \psi \in [-180^\circ, 180^\circ]$  or  $[-\pi, \pi)$ ,

$$\mathcal{R}(\phi, \psi) = \frac{\phi + \psi + 2\pi}{4\pi}. \quad (9)$$

372 Conformation of this limit is shown numerically in Fig. 13. Since larger  $\sigma$ s indicate higher accuracy,  
373  $\lim_{\sigma \rightarrow \infty} \mathcal{R}(\phi, \psi)$  represents an exact representation of the Ramachandran number. Using this closed form,  
374 this report shows how both static structural features and complex structural transitions may be identified  
375 with the help of Ramachandran number-derived plots.

Assuming, a different range (say,  $\phi, \psi \in [0, 2\pi)$ ), the Ramachandran number in that frame of reference will be

$$\mathcal{R}(\phi, \psi)_{\phi, \psi \in [0, 2\pi)} = \frac{\phi + \psi}{4\pi}. \quad (10)$$

376 However, in changing the ranges, the meaning of the Ramachandran number will change. This manuscript  
377 assumes that all angles  $(\phi, \psi, \omega)$  range between  $-\pi$  ( $-180^\circ$ ) and  $\pi$  ( $180^\circ$ )

## 378 REFERENCES

- 379 **Alberts B, Johnson A, Lewis J, Raff M, Roberts K, Walter P. 2002.** Molecular biology of the cell.  
380 new york: Garland science; 2002. *Classic textbook now in its 5th Edition* .
- 381 **Baruah A, Rani P, Biswas P. 2015.** Conformational entropy of intrinsically disordered proteins from  
382 amino acid triads. *Scientific reports* 5.
- 383 **Beck DA, Alonso DO, Inoyama D, Daggett V. 2008.** The intrinsic conformational propensities of the  
384 20 naturally occurring amino acids and reflection of these propensities in proteins. *Proceedings of the*  
385 *National Academy of Sciences* 105(34):12259–12264.
- 386 **Berg JM, Tymoczko JL, Stryer L. 2010.** *Biochemistry, International Edition*. WH Freeman & Co.,  
387 New York, 7 edition.
- 388 **Chebrek R, Leonard S, de Brevern AG, Gelly JC. 2014.** Polyproline: polyproline helix ii and  
389 secondary structure assignment database. *Database* 2014:bau102.
- 390 **Dunker A, Babu M, Barbar E, Blackledge M, Bondos S, Dosztányi Z, Dyson H, Forman-Kay J,  
391 Fuxreiter M, Gsponer J, Han KH, Jones D, Longhi S, Metallo S, Nishikawa K, Nussinov R,  
392 Obradovic Z, Pappu R, Rost B, Selenko P, Subramaniam V, Sussman J, Tompa P, Uversky V.  
393 2013.** What's in a name? why these proteins are intrinsically disordered? *Intrinsically Disordered*  
394 *Proteins* 1:e24157.
- 395 **Espinoza-Fonseca LM. 2009.** Reconciling binding mechanisms of intrinsically disordered proteins.  
396 *Biochemical and biophysical research communications* 382(3):479–482.
- 397 **Fink AL. 2005.** Natively unfolded proteins. *Curr Opin Struct Biol* 15(1):35–41.
- 398 **Fox NK, Brenner SE, Chandonia JM. 2014.** Scope: Structural classification of proteins—extended,  
399 integrating scop and astral data and classification of new structures. *Nucleic Acids Res* 42(Database  
400 issue):D304–D309. doi:10.1093/nar/gkt1240.

- 401 **Frishman D, Argos P. 1995.** Knowledge-based protein secondary structure assignment. *Proteins:*  
402 *Structure, Function, and Bioinformatics* **23(4)**:566–579.
- 403 **Geist L, Henen MA, Haiderer S, Schwarz TC, Kurzbach D, Zawadzka-Kazimierczuk A, Saxena**  
404 **S, Źerko S, Koźmiński W, Hinderberger D, et al. 2013.** Protonation-dependent conformational  
405 variability of intrinsically disordered proteins. *Protein Science* **22(9)**:1196–1205.
- 406 **Gunasekaran K, Nagarajaram H, Ramakrishnan C, Balaram P. 1998.** Stereochemical punctuation  
407 marks in protein structures: glycine and proline containing helix stop signals. *Journal of molecular*  
408 *biology* **275(5)**:917–932.
- 409 **Ho BK, Brasseur R. 2005.** The ramachandran plots of glycine and pre-proline. *BMC structural biology*  
410 **5(1)**:1.
- 411 **Hoof RW, Sander C, Vriend G. 1997.** Objectively judging the quality of a protein structure from a  
412 ramachandran plot. *Computer applications in the biosciences: CABIOS* **13(4)**:425–430.
- 413 **Humphrey W, Dalke A, Schulten K. 1996.** VMD – Visual Molecular Dynamics. *Journal of Molecular*  
414 *Graphics* **14**:33–38.
- 415 **James LC, Tawfik DS. 2003a.** Conformational diversity and protein evolution—a 60-year-old hypothesis  
416 revisited. *Trends Biochem Sci* **28(7)**:361–368.
- 417 **James LC, Tawfik DS. 2003b.** The specificity of cross-reactivity: promiscuous antibody binding involves  
418 specific hydrogen bonds rather than nonspecific hydrophobic stickiness. *Protein Sci* **12(10)**:2183–2193.
- 419 **Kabsch W, Sander C. 1983.** Dictionary of protein secondary structure: pattern recognition of hydrogen-  
420 bonded and geometrical features. *Biopolymers* **22(12)**:2577–2637. doi:10.1002/bip.360221211.
- 421 **Kosol S, Contreras-Martos S, Cedeño C, Tompa P. 2013.** Structural characterization of intrinsically  
422 disordered proteins by nmr spectroscopy. *Molecules* **18(9)**:10802–10828.
- 423 **Laskowski RA. 2003.** Structural quality assurance. *Structural Bioinformatics, Volume 44* pages 273–303.
- 424 **Laskowski RA, MacArthur MW, Moss DS, Thornton JM. 1993.** Procheck: a program to check the  
425 stereochemical quality of protein structures. *Journal of applied crystallography* **26(2)**:283–291.
- 426 **Lovell SC, Davis IW, Arendall WB, de Bakker PIW, Word JM, Prisant MG, Richardson JS,**  
427 **Richardson DC. 2003.** Structure validation by Calpha geometry: phi,psi and Cbeta deviation. *Proteins*  
428 **50(3)**:437–450. ISSN 1097-0134. doi:10.1002/prot.10286.
- 429 **Mannige RV. 2014.** Dynamic new world: Refining our view of protein structure, function and evolution.  
430 *Proteomes* **2(1)**:128–153.
- 431 **Mannige RV. 2017.** An exhaustive survey of regular peptide conformations using a new metric for  
432 backbone handedness (*h*). *PeerJ* **5**:e3327. ISSN 2167-8359. doi:10.7717/peerj.3327.
- 433 **Mannige RV, Haxton TK, Proulx C, Robertson EJ, Battigelli A, Butterfoss GL, Zuckermann RN,**  
434 **Whitelam S. 2015.** Peptoid nanosheets exhibit a new secondary structure motif. *Nature* **526**:415–420.
- 435 **Mannige RV, Kundu J, Whitelam S. 2016.** The Ramachandran number: an order parameter for protein  
436 geometry. *PLoS One* **11(8)**:e0160023.
- 437 **Midic U, Oldfield CJ, Dunker AK, Obradovic Z, Uversky VN. 2009.** Protein disorder in the human  
438 diseasome: unfoldomics of human genetic diseases. *BMC Genomics* **10 Suppl 1**:S12. doi:10.1186/  
439 1471-2164-10-S1-S12.
- 440 **Momen R, Azizi A, Wang L, Yang P, Xu T, Kirk SR, Li W, Manzhos S, Jenkins S. 2017.** The role  
441 of weak interactions in characterizing peptide folding preferences using a qtaim interpretation of the  
442 ramachandran plot ( $\phi$ - $\psi$ ). *International Journal of Quantum Chemistry* .
- 443 **Oldfield CJ, Cheng Y, Cortese MS, Brown CJ, Uversky VN, Dunker AK. 2005.** Comparing and  
444 combining predictors of mostly disordered proteins. *Biochemistry* **44(6)**:1989–2000.
- 445 **Ramachandran G, Ramakrishnan C, Sasisekharan V. 1963.** Stereochemistry of polypeptide chain  
446 configurations. *Journal of molecular biology* **7(1)**:95–99.
- 447 **Schad E, Tompa P, Hegyi H. 2011.** The relationship between proteome size, structural disorder and  
448 organism complexity. *Genome Biol* **12(12)**:R120.
- 449 **Sibille N, Bernardo P. 2012.** Structural characterization of intrinsically disordered proteins by the  
450 combined use of nmr and saxs. *Biochemical society transactions* **40(5)**:955–962.
- 451 **Subramanian E. 2001.** Gn ramachandran. *Nature Structural & Molecular Biology* **8(6)**:489–491.
- 452 **Tien MZ, Sydykova DK, Meyer AG, Wilke CO. 2013.** Peptidebuilder: A simple python library to  
453 generate model peptides. *PeerJ* **1**:e80.
- 454 **Ting D, Wang G, Shapovalov M, Mitra R, Jordan MI, Dunbrack RL Jr. 2010.** Neighbor-dependent  
455 ramachandran probability distributions of amino acids developed from a hierarchical dirichlet process

456 model. *PLOS Computational Biology* **6(4)**:1–21. doi:10.1371/journal.pcbi.1000763.  
457 **Tokuriki N, Tawfik DS. 2009.** Protein dynamism and evolvability. *Science* **324(5924)**:203–207.  
458 **Tompa P. 2011.** Unstructural biology coming of age. *Curr Opin Struct Biol* **21(3)**:419–425. doi:  
459 10.1016/j.sbi.2011.03.012.  
460 **Uversky VN. 2003.** Protein folding revisited. a polypeptide chain at the folding-misfolding-nonfolding  
461 cross-roads: which way to go? *Cell Mol Life Sci* **60(9)**:1852–1871.  
462 **Uversky VN, Dunker AK. 2010.** Understanding protein non-folding. *Biochim Biophys Acta*  
463 **1804(6)**:1231–1264.  
464 **Vértessy BG, Orosz F. 2011.** From “fluctuation fit” to “conformational selection”: evolution, rediscovery,  
465 and integration of a concept. *Bioessays* **33(1)**:30–34.